PAPER

Induction of smectic polymorphism in bent-core derivatives of the 6-oxoverdazyl by partial fluorination of alkyl chains†

Sylwia Ciastek,[a] Piotr Kaszyński,*[abc] Damian Pociecha[d] and Marcin Jasiński[a]

A series of bent-core mesogens 2[m,n] derived from the 6-oxoverdazyl radical and containing partially fluorinated alkyl tails was prepared and investigated by thermal, optical, XRD and EPR methods. In contrast to non-fluorinated analogs, the series 2[m,n] exhibits SmA and SmC phases with thermal stability dependent on the degree of fluorination and the F/H ratio (m/n) in the alkyl chain.

Introduction

With the increasing number and variety of all-organic paramagnetic liquid crystals[1] the focus is shifting towards optimization of their properties for specific applications. Materials based on π-delocalized radicals are of particular interest in the context of molecular electronics and spintronics[2] due to their photophysical and electrochemical properties.[3] In this context we have been working with 6-oxoverdazyl and demonstrated that it is a suitable paramagnetic structural element for disc-like[4–9] and bent-core, such as 1[n] (Fig. 1),[10,11] liquid crystalline materials. The latter compounds exhibit ambipolar photoconductivity, electro-optical effects, a novel Tet$_{3D}$ phase,[10] and their electronic absorption covers the visible region of the spectrum depending on the substituent at the C(3) position.[11] The bent-core mesogens 1[n] typically exhibit a nematic phase. For electronic applications, however, more organized lamellar phases with close intermolecular contacts are necessary. As the first step towards this goal we have focused on fluorofobic[12] interactions to induce nanosegregation.[13] In this context we have investigated a series of mesogens 2[m,n] bearing partially fluorinated alkyl chains (Fig. 1).

Here we discuss the synthesis, thermal and optical investigation of series 2[m,n], and analysis of mesophases by powder XRD and EPR methods.
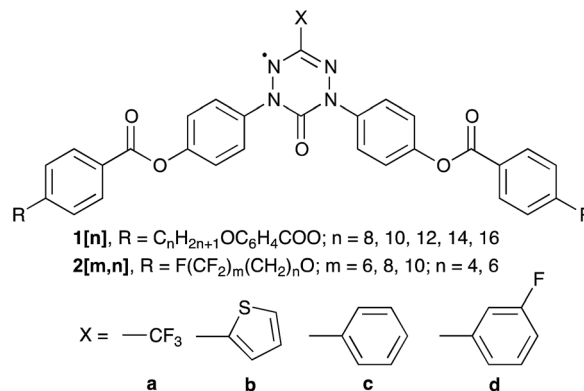
[a]Faculty of Chemistry, University of Łódź, Tamka 12, 91-403 Łódź, Poland. E-mail: piotrk@cbmm.lodz.pl
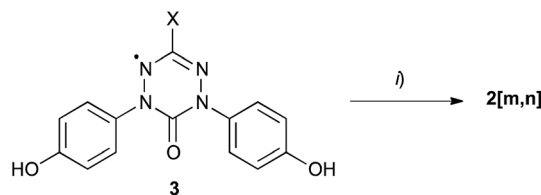
[b]Organic Materials Research Group, Centre of Molecular and Macromolecular Studies, Polish Academy of Sciences, Sienkiewicza 112, 90-363 Łódź, Poland

[c]Department of Chemistry, Middle Tennessee State University, Murfreesboro, TN, 37130, USA

[d]Department of Chemistry, University of Warsaw, Żwirki i Wigury 101, 02-089 Warsaw, Poland

† Electronic supplementary information (ESI) available. See DOI: 10.1039/c6ra21383a

Results and discussion

Synthesis

6-Oxoverdazyl derivatives 2[m,n] were obtained in yields 57–82% by esterification of diphenols 3 with appropriate 4-alkoxybenzoyl chlorides 4[m,n] in the presence of DMAP (Scheme 1). The diphenol precursors 3 were obtained using the general Milcent protocol[14] following functional group transformations,[15] as described recently.[11] The required benzoyl chlorides 4[m,n] were prepared from the corresponding 4-alkoxybenzoic acids[16] and SOCl$_2$.

Thermal analysis

Optical microscopy and DSC analysis revealed that all derivatives in series 2[m,n] exhibit liquid crystalline behavior, with the exception of 2[6,4]a (Table 1). Thus, all mesogens form a SmA phase, while in derivatives 2[m,n]a (X = CF$_3$) also a monotropic SmC phase was detected by optical microscopy (Fig. 2 and 3) and confirmed by powder XRD (vide infra). This is in sharp contrast with behavior found in the non-fluorinated series 1[n]: only the shortest member of the 1[n]a series, derivative 1[8]a,

1[n], R = C$_n$H$_{2n+1}$OC$_6$H$_4$COO; n = 8, 10, 12, 14, 16
2[m,n], R = F(CF$_2$)$_m$(CH$_2$)$_n$O; m = 6, 8, 10; n = 4, 6

X = —CF$_3$

a   b   c   d

Fig. 1 The structures of bent-core 6-oxoverdazyls 1[n] and 2[m,n].

Scheme 1 Preparation of 6-oxoverdazyls **2[m,n]**. Reagents and conditions: (i) $F(CF_2)_m(CH_2)_nOC_6H_4COCl$ (**4[m,n]**), DMAP, CH_2Cl_2, rt.

Fig. 2 A DSC trace of **2[8,4]a**; heating/cooling rates are 10 K min^{-1}.

exhibits a monotropic SmA phase,[10] while other derivatives show nematic and tetragonal phases or no mesogenic behavior at all (**1[n]b** and **1[n]c**).[10,11] Thus, it appears that removal of the –C_6H_4COO– group and partial fluorination of the alkoxy chain in **1[n]** is an effective tool for induction of a broad-range mesogenic behavior in 6-oxoverdazyls **2[m,n]** irrespectively on the nature of substituent X at the C(3) position. For example, while the thien-2-yl derivative **1[12]b** melts at 153 °C and has a virtual N–I transition ($[T_{NI}]$) at 138 °C,[11] the fluorocarbon analogue **2[6,6]b** exhibits a SmA phase between 107 °C and 197 °C (Table 1).

Analysis of data in Table 1 demonstrates that the meso-phase stability strongly depends on the size of the semirigid perfluoroalkane segment. For instance, increasing the number of the CF_2 units from 6 to 8 induces smectic behavior in **2[8,4]a**, and additional two CF_2 units increase SmA and SmC phase stability by about 30 K in **2[10,4]a** with a modest increase of melting temperature. Similar behavior is observed in the pair **2[6,6]a** and **2[8,6]a** in which elongation of the fluorocarbon by two units results in stabilization of the SmA phase by nearly 60 K.

Data in Table 1 also permits analysis of the effect of the degree of alkyl chain fluorination on transition temperatures. Thus, increasing the number of fluorine atoms or changing the F/H ratio in the C_{12} chain from 1 : 1 in **2[6,6]a** to 2 : 1 in **2[8,4]a** increases the SmA–I transition temperature by 59 K. In another pair with the C_{14} tail (**2[8,6]a** and **2[10,4]a**), changing the F/H ratio from 4 : 3 to 5 : 2 increases SmA phase stability by 34 K.

Finally a comparison of derivatives in series **2[6,6]** demonstrates that the effectiveness of the C(3)–X substituent in stabilization of the SmA follows the order $CF_3 < C_6H_5 < C_6H_4F$-m < 2-thienyl, which is different from that established for the virtual N–I transition temperature in series **1[12]**:[11] 2-thienyl < $CF_3 < C_6H_5 < C_6H_4F$-m. This stark difference in the position of the 2-thienyl substituent in the two series suggests that other molecular factors, such as the π–π interactions, are important in the stabilization of the nematic and smectic phases.

Powder XRD analysis

XRD analysis confirmed the presence of a SmA phase in all mesogenic compounds in series **2[m,n]** and a SmC phase in derivatives **2[m,n]a** (see the ESI,† and X-ray diffractogram for **2[8,4]a** in Fig. 4). All compounds exhibit a typical layer thickness dependence on temperature: it increases in SmA phase and then decreases in the SmC phase with decreasing temperature. Analysis of the thermal expansion coefficient κ, obtained by fitting the datapoints to a quadratic function $d_{01} = \kappa T^2 + b$, demonstrates that the layer thickness change depends on the substituent at the C(3) position: it is similar for the aryl groups and twice larger for

Table 1 Thermal properties of **2[m,n]**[a]

Compound	$(CF_2)_m$	$(CH_2)_n$	X	Transition temperatures/°C
2[6,4]a	6	4	CF_3	Cr 156 I
2[6,6]a	6	6	CF_3	Cr 132 (SmC 75 SmA 91)[b] I
2[8,4]a	8	4	CF_3	Cr 127 (SmC 108)[b] SmA 150 I
2[8,6]a	8	6	CF_3	Cr 124 (SmC 116)[b] SmA 149 I
2[10,4]a	10	4	CF_3	Cr 144 (SmC 137)[b] SmA 183 I
2[6,6]b	6	6	Th	Cr 107 SmA 197 I[c]
2[8,4]b	8	4	Th	Cr 129 SmA 245 I[c,d]
2[10,4]b	10	4	Th	Cr 136 SmA ~220 I[c,d]
2[6,6]c	6	6	Ph	Cr 135 SmA 183 I
2[6,6]d	6	6	3-FC_6H_4	Cr 147 SmA 192 I

[a] Cr = crystal, SmA = smectic A, SmC = smectic C, I = isotropic. Typical heating rate 10 K min^{-1}. [b] Monotropic transition. Temperatures from XRD analysis. [c] Decomposition. [d] Heating rate 35 K min^{-1}.
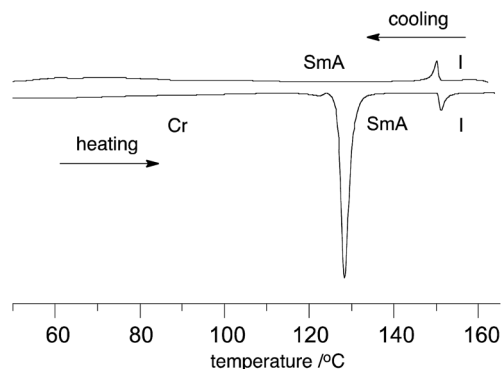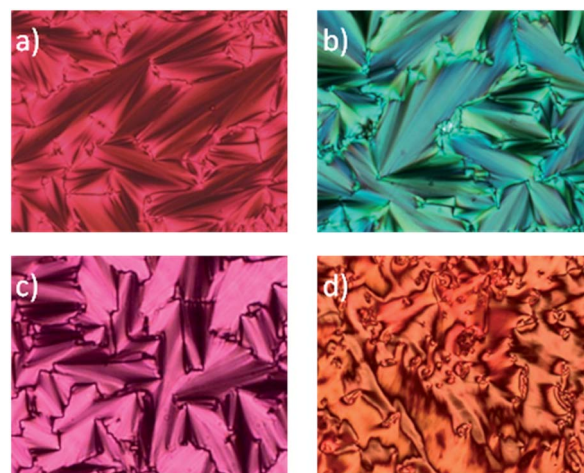

Fig. 3 Optical textures of a SmA phase in **2[6,6]c** (a), **2[6,6]b** (b), **2[8,6]a** (c), and a schlieren texture of a SmC phase in **2[8,6]a** (d; without top cover) obtained on slow cooling from the isotropic phase.
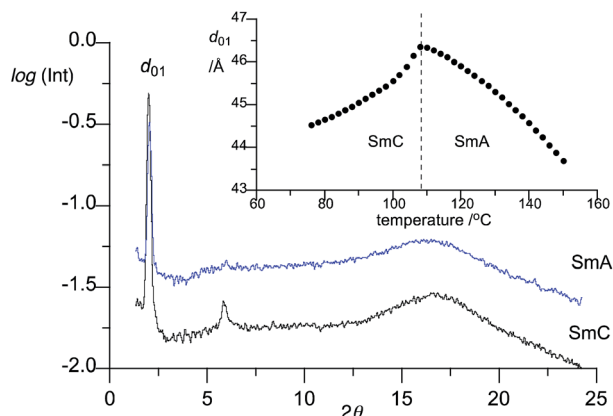
Fig. 4 X-ray diffractogram for SmA and SmC phases of **2[8,4]a** at 140 °C and 100 °C, respectively, obtained by integration of the 2D patterns. The insert shows temperature dependence of the d_{01} signal.

the CF_3 group and follows the order: 2-thienyl < $C_6H_5 \sim C_6H_4F$-m < CF_3 (Table 2). This indicates that derivatives **2[m,n]a** undergo the most substantial molecular reorganization in the SmA phase presumably due to the bulk of the CF_3 substituent. Conversely, least reorganization in the SmA phase is observed in the thienyl derivative **2[6,6]b**, which coincides with its highest SmA–I transition temperature in the series (Table 1).

Data in Table 2 also suggests that the higher degree of fluorination in the alkyl tail (longer R_f component or higher F/H ratio) the stronger temperature effect on the layer thickness.

A comparison of the layer thickness with DFT-calculated molecular size indicates a partial (up to 20%) interdigitation of the molecules in the SmA phase as shown for **2[6,6]b** in Fig. 5.

The typical lack of intralayer molecular correlation in the observed SmA and SmC phases is consistent with no photoconductivity observed in a sample of **2[8,4]a**.

EPR analysis

In contrast to standard SQUID magnetometry, EPR spectroscopy provides information on local spin–spin interactions in
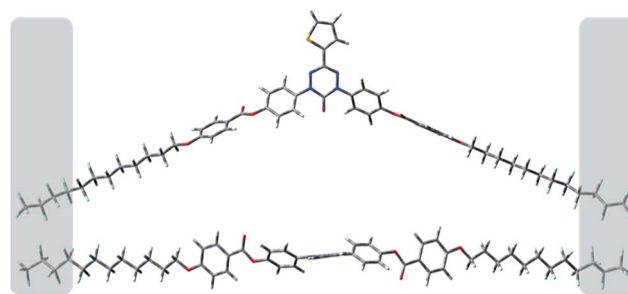
Table 2 Layer spacing d_{01}, molecular length L, degree of interdigitation I, and thermal expansion coefficient κ

	SmA				SmC
Compound	$d_{01}{}^a$/Å	L^b/Å	I^c/%	κ^d/pm K^{-2}	$d_{01}{}^e$/Å
2[6,6]a	45.07	54.14	17	−0.031	43.27
2[8,4]a	44.57	53.46	17	−0.026	45.56
2[8,6]a	47.11	57.93	19	−0.039	47.99
2[10,4]a	47.18	58.66	20	−0.033	50.18
2[6,6]b	44.75	53.97	17	−0.015	—
2[6,6]c	44.28	53.99	18	−0.017	—
2[6,6]d	44.30	53.99	18	−0.017	—

^{a} Layer spacing measured at $T = T_{AI} - 10$ K. ^{b} The length of the molecule measured as the F···F distance. ^{c} Degree of interdigitation $I = (L - d_{01})/L$. ^{d} Thermal expansion coefficient for the SmA phase from the fitting the $\kappa T^2 + b$ function. See the ESI. ^{e} Layer spacing measured at $T = T_{AC} - 6$ K.

Fig. 5 Two views of **2[6,6]b** modelled at the B3LYP/6-31G* level of theory. The shaded areas suggest interdigitated parts of the molecule.
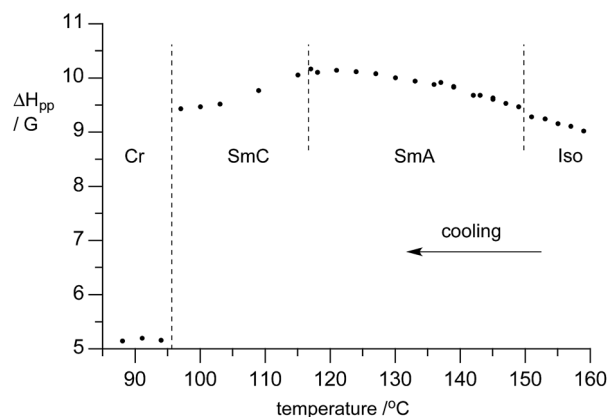

Fig. 6 EPR line width as a function of temperature recorded for neat **2[8,6]a** on cooling.

a greater temperature range and is suitable for studying of high temperature paramagnetic liquid crystals,[17] such as series **2[m,n]**. Thus, analysis of **2[8,6]a** demonstrated a monotonic broadening of the single line EPR spectrum with decreasing temperature resulting from increasing spin–spin exchange interactions in the neat isotropic phase (Fig. 6). At the I–SmA transition increased molecular organization in the lamellar structure results in a subtle increase of the line width (ΔH_{pp}). Maximum line width is observed for the SmA phase just before the SmA–SmC transition at 116 °C at which the phase has the highest order. In the SmC phase the line width, ΔH_{pp}, decreases due to progressing molecular tilt and changing spin–spin exchange interactions. At 96 °C the monotropic SmC phase crystallizes abruptly changing the strength of spin–spin interactions between the paramagnetic centres in the rigid crystalline phase. Thus, the variable temperature EPR spectroscopy offers a convenient tool for analysis of molecular organization in fluid phases.[17]

Conclusions

Partial fluorination of the alkyl chains in bent-core derivatives of 6-oxoverdazyl **1[n]** induced SmA and SmC behavior in series **2[m,n]**; unfortunately, more organized lamellar phases desired for electronic applications were not observed. The mesophase stability in the series depends on the degree of alkyl chain

fluorination, and increases with increasing size of the perfluoroalkyl segment.

Variable temperature EPR was demonstrated to be a useful tool in studying of local spin–spin interactions as a function of the phase structure. The search for banana phases in the 6-oxoverdazyl derivatives with intralayer molecular correlation continues.

Computational details

Quantum-mechanical calculations were carried out using Gaussian 09 suite of programs.[18] Geometry optimizations for unconstrained molecules at the pseudo-C_2 symmetry were undertaken at the B3LYP/6-31G* level of theory using default convergence limits.

Experimental section

General

Solvents and reagents were purchased and used as received without further purification. Products were purified by flash chromatography on silica gel (230–400 mesh, Merck or Fluka). IR spectra were measured in KBr pellets with a FT-IR NEXUS spectrometer. Mass spectrometry was performed with a Finnigan MAT-95 or a Varian 500-MS LC Ion Trap instrument. Thermal analysis was performed with differential scanning calorimeter DSC-1 Mettler Toledo and onset temperatures are reported in Table 1.

X-ray diffraction experiments in the wide-angle range were performed with Bruker D8 GADDS system, and Bruker Nanostar system was used for small angle diffraction measurements.

Variable temperature EPR spectra for neat radical **2[8,6]a** were recorded using an X-band Bruker spectrometer every 2–3 K on cooling allowing for 2 min stabilization. The line width was measured as a difference in position of the maximum and minimum of the EPR signal.

If not stated otherwise, reactions were carried out under argon in a flame-dried flask with addition of the reactants *via* syringe; subsequent manipulations were conducted in air.

The synthesis of diphenols **3** was reported recently.[11]

Synthesis of 6-oxoverdazyls 2[*m*,*n*]. A mixture of diphenol **3** (0.23 mmol) and freshly prepared appropriate acid chloride **4[*m*,*n*]** (0.57 mmol) in dry CH_2Cl_2 (5 mL) containing DMAP (84 mg, 0.69 mmol) was stirred at room temperature until the diphenol and the intermediate mono-acylated derivative were fully consumed (about 20–30 min). The mixture was quenched with H_2O, and the products extracted with CH_2Cl_2 (3 × 10 mL). The organic layers were dried ($MgSO_4$), and the solvents were removed under reduced pressure. The resulting crude product was purified by chromatography followed by repeated recrystallization. Reported yields refer to analytically pure samples.

1,5-Bis{4-[4-(5,5,6,6,7,7,8,8,9,9,10,10,10-tridecafluoro-decyloxy)-benzoyloxy]phenyl}-3-trifluoromethyl-6-oxoverdazyl (2[6,4]a). Crude product was purified by column chromatography (SiO_2, CH_2Cl_2/petroleum ether 2 : 1) followed by recrystallization (CH_3CN, 3×) to yield 215 mg (70%) as wine-red crystals: IR (KBr) ν 1734 (C=O), 1606, 1512, 1498 (C=C), 1256, 1201, 1165, 1144 (C–F), 1067 (C–O)

cm^{-1}; MALDI-MS (*m/z*): 1311.3 (100, $[M - CO]^+$). Anal. calcd for $C_{49}H_{32}F_{29}N_4O_7$: C, 43.93; H, 2.41; N, 4.18. Found: C, 44.01; H, 2.45; N, 4.07.

1,5-Bis{4-[4-(5,5,6,6,7,7,8,8,9,9,10,10,11,11,12,12,12-heptadeca-fluorododecyloxy)benzoyloxy]phenyl}-3-trifluoromethyl-6-oxoverdazyl (2[8,4]a). Crude product was purified by column chromatography (SiO_2, CH_2Cl_2/petroleum ether 2 : 1) followed by recrystallization (CH_3CN, 3×) to yield 231 mg (66%) as orange crystals: IR (KBr) ν 1729 (C=O), 1607, 1511 (C=C), 1257, 1205, 1167 (C–F) cm^{-1}; MALDI-MS (*m/z*): 1511.3 (100, $[M - CO]^+$). Anal. calcd for $C_{53}H_{32}F_{37}N_4O_7$: C, 41.34; H, 2.09; N, 3.64. Found: C, 41.42; H, 2.07; N, 3.46.

1,5-Bis{4-[4-(5,5,6,6,7,7,8,8,9,9,10,10,11,11,12,12,13,13,14,14,14-henicosafluorotetradecyloxy)benzoyloxy]phenyl}-3-trifluoromethyl-6-oxoverdazyl (2[10,4]a). Crude product was purified by column chromatography (SiO_2, CH_2Cl_2/petroleum ether 1 : 1 gradient 3 : 1) followed by recrystallization (CH_3CN, 5×) to yield 173 mg (58%) as orange crystals: MALDI-MS (*m/z*): 1711.1 (100, $[M - CO]^+$). Anal. calcd for $C_{57}H_{32}F_{45}N_4O_7$: C, 39.35; H, 1.85; N, 3.22. Found: C, 39.34; H, 2.10; N, 2.99.

1,5-Bis{4-[4-(7,7,8,8,9,9,10,10,11,11,12,12,12-tridecafluoro-dodecyloxy)benzoyloxy]phenyl}-3-trifluoromethyl-6-oxoverdazyl (2[6,6]a). Crude product was purified by column chromatography (SiO_2, CH_2Cl_2/petroleum ether 2 : 1.5) followed by recrystallization (AcOEt/CH_3CN, 1 : 4 and AcOEt/pentane, 1 : 4; 3×) to yield 205 mg (63%) as orange crystals: IR (KBr) ν 1733 (C=O), 1606, 1511 (C=C), 1254, 1068 (C–O), 1203, 1166, 1146 (C–F), 1068 (C–O) cm^{-1}; MALDI-MS (*m/z*): 1367.4 (100, $[M - CO]^+$). Anal. calcd for $C_{53}H_{40}F_{29}N_4O_7$: C, 45.60; H, 2.89; N, 4.01. Found: C, 45.89; H, 3.14; N, 3.88.

1,5-Bis{4-[4-(7,7,8,8,9,9,10,10,11,11,12,12,13,13,14,14,14-hepta-decafluorotetradecyloxy)benzoyloxy]phenyl}-3-trifluoromethyl-6-oxoverdazyl (2[8,6]a). Crude product was purified by column chromatography (SiO_2, CH_2Cl_2/petroleum ether 2 : 1) followed by recrystallization (CH_3CN, 3×) to yield 260 mg (72%) as orange crystals: IR (KBr) ν 1729 (C=O), 1607, 1510 (C=C), 1255, 1205, 1150, 1167 (C–F), 1074 (C–O) cm^{-1}; MALDI-MS (*m/z*): 1567.6 (100, $[M - CO]^+$). Anal. calcd for $C_{57}H_{40}F_{37}N_4O_7$: C, 42.90; H, 2.59; N, 3.51. Found: C, 42.98; H, 2.48; N, 3.24.

1,5-Bis{4-[4-(7,7,8,8,9,9,10,10,11,11,12,12,12-tridecafluoro-dodecyloxy)benzoyloxy]phenyl}-3-thien-2-yl-6-oxoverdazyl (2[6,6]b). Crude product was purified by column chromatography (SiO_2, CH_2Cl_2/hexane 10 : 1) followed by recrystallization (AcOEt/pentane, 1 : 5 and AcOEt/CH_3CN, 1 : 5; 4×) to yield 175 mg (62%) as dark green crystals: IR (KBr) ν 1734 (C=O), 1607, 1511 (C=C), 1257 (C–O), 1204, 1166, 1145 (C–F), 1069 (C–O) cm^{-1}; MALDI-MS (*m/z*): 1381.1 (100, $[M - CO]^+$). Anal. calcd for $C_{56}H_{43}F_{26}N_4O_7S$: C, 47.70; H, 3.07; N, 3.97. Found: C, 47.77; H, 3.27; N, 3.68.

1,5-Bis{4-[4-(5,5,6,6,7,7,8,8,9,9,10,10,11,11,12,12,12-heptadeca-fluorododecyloxy)benzoyloxy]phenyl}-3-thien-2-yl-6-oxoverdazyl (2[8,4]b). Crude product was purified by column chromatography (Al_2O_3, petroleum ether/AcOEt 10 : 1 gradient 3 : 1) followed by recrystallization (CH_2Cl_2/pentane, 1 : 6; 5×) to yield 190 mg (60%) as green crystals; IR (KBr) ν 1736 (C=O), 1692, 1609, 1511 (C=C), 1261 (C–O), 1207, 1166, 1147 (C–F), 1074 (C–O) cm^{-1}; MALDI-MS (*m/z*): 1525.2 (100, $[M - CO]^+$). Anal. calcd

for $C_{56}H_{35}F_{34}N_4O_7S$: C, 43.28; H, 2.27; N, 3.61. Found: C, 43.20; H, 2.20; N, 3.34.

1,5-Bis{4-[4-(5,5,6,6,7,7,8,8,9,9,10,10,11,11,12,12,13,13,14,14,14-henicosafluorotetradecyloxy)benzoyloxy]phenyl}-3-thien-2-yl-6-oxoverdazyl (2[10,4]b). Crude product was purified by column chromatography (Al_2O_3, petroleum ether/AcOEt 10 : 1 gradient 3 : 1) followed by recrystallization (CH_2Cl_2/pentane, 1 : 4 and CH_2Cl_2/CH_3CN, 1 : 4; 5×) to yield 150 mg (57%) as green crystals: IR (KBr) ν 1733 (C=O), 1695, 1609, 1513 (C=C), 1255 (C–O), 1211, 1166, 1154 (C–F), 1071 (C–O) cm^{-1}; MALDI-MS (m/z): 1725.2 (100, [M – CO]$^+$). Anal. calcd for $C_{60}H_{35}F_{42}N_4O_7S$: C, 41.09; H, 2.01; N, 3.19; S, 1.83. Found: C, 41.05; H, 2.27; N, 3.03; S, 1.99.

1,5-Bis{4-[4-(7,7,8,8,9,9,10,10,11,11,12,12,12-tridecafluorododecyloxy)benzoyloxy]phenyl}-3-phenyl-6-oxoverdazyl (2[6,6]c). Crude product was purified by column chromatography (SiO_2, CH_2Cl_2/petroleum ether 7 : 1 gradient 1 : 0) followed by recrystallization (AcOEt/CH_2Cl_2, 1 : 4 and CH_3CN; 4×) to yield 170 mg (75%) as green-grey crystals: IR (KBr) ν 1740 (C=O), 1695, 1606, 1510 (C=C), 1251 (C–O), 1204, 1168, 1144 (C–F), 1073 (C–O) cm^{-1}; MALDI-MS (m/z): 1375.4 (100, [M – CO]$^+$). Anal. calcd for $C_{58}H_{45}F_{26}N_4O_7$: C, 49.62; H, 3.23; N, 3.99. Found: C, 49.42; H, 3.31; N, 3.78.

1,5-Bis{4-[4-(7,7,8,8,9,9,10,10,11,11,12,12,12-tridecafluorododecyloxy)benzoyloxy]phenyl}-3-(3-fluorophenyl)-6-oxoverdazyl (2[6,6]d). Crude product was purified by column chromatography (SiO_2, CH_2Cl_2/petroleum ether 8 : 1 gradient 1 : 0) followed by recrystallization (CH_3CN/AcOEt, 3 : 1; 3×) to yield 121 mg (82%) as pink-red crystals: IR (KBr) ν 1734 (C=O), 1691, 1607, 1511 (C=C), 1258 (C–O), 1206, 1167, 1145 (C–F), 1071 (C–O) cm^{-1}; MALDI-MS (m/z): 1393.0 (100, [M – CO]$^+$). Anal. calcd for $C_{58}H_{44}F_{27}N_4O_7$: C, 48.99; H, 3.12; N, 3.94. Found: C, 48.85; H, 3.09; N, 3.66.

Preparation of acid chlorides 4[m,n]. A solution of 4-substituted benzoic acid[16] (0.57 mmol) and $SOCl_2$ (4.5 mL) was refluxed for 20 min. Excess thionyl chloride was removed under vacuum. The remaining precipitate was dissolved in dry CH_2Cl_2, the solvent was evaporated, and the procedure was repeated 2 times to remove traces $SOCl_2$. The resulting colorless solid was dried under vacuum until no more odor of $SOCl_2$ was detected, and used immediately for the subsequent esterification reaction.

Acknowledgements

References

1 R. Tamura, Y. Uchida and K. Suzuki, in *Handbook of Liquid Crystals*, J. W. Goodby, P. J. Collings, T. Kato, C. Tschierske, H. F. Gleeson and P. Raynes, ed. Wiley-VCH, Weinheim, 2014, vol. 8, pp. 837–864.

2 P. Ravat, T. Marszalek, W. Pisula, K. Müllen and M. Baumgarten, *J. Am. Chem. Soc.*, 2014, **136**, 12860–12863.

3 *Stable radicals: fundamentals and applied aspects of odd-electron compounds*, ed. R. G. Hicks, John Wiley & Sons, Chichester, 2010.

4 A. Jankowiak, D. Pociecha, H. Monobe, J. Szczytko, Ż. Dębska, J. Romański and P. Kaszyński, *Phosphorus, Sulfur Silicon Relat. Elem.*, 2013, **188**, 418–426.

5 A. Jankowiak, D. Pociecha, H. Monobe, J. Szczytko and P. Kaszyński, *Chem. Commun.*, 2012, **48**, 7064–7066.

6 A. Jankowiak, D. Pociecha, J. Szczytko and P. Kaszyński, *Liq. Cryst.*, 2014, **41**, 1653–1660.

7 A. Jankowiak, D. Pociecha, J. Szczytko, H. Monobe and P. Kaszyński, *J. Am. Chem. Soc.*, 2012, **134**, 2465–2468.

8 A. Jankowiak, D. Pociecha, J. Szczytko, H. Monobe and P. Kaszyński, *J. Mater. Chem. C*, 2014, **2**, 319–324.

9 A. Jankowiak, D. Pociecha, J. Szczytko, H. Monobe and P. Kaszyński, *Liq. Cryst.*, 2014, **41**, 385–392.

10 M. Jasiński, D. Pociecha, H. Monobe, J. Szczytko and P. Kaszyński, *J. Am. Chem. Soc.*, 2014, **136**, 14658–14661.

11 S. Ciastek, M. Jasiński and P. Kaszyński, *RSC Adv.*, 2015, **5**, 33328–33333.

12 C. Tschierske, *Top. Curr. Chem.*, 2012, **318**, 1–108.

13 C. Tschierske, in *Handbook of Liquid Crystals*, ed. J. W. Goodby, P. J. Collings, T. Kato, C. Tschierske, H. F. Gleeson and P. Raynes, Wiley-VCH, Weinheim, 2014, vol. 5, pp. 1–43, and references therein.

14 R. Milcent, G. Barbier, S. Capelle and J.-P. Catteau, *J. Heterocycl. Chem.*, 1994, **31**, 319–324.

15 M. Jasiński, J. S. Gerding, A. Jankowiak, K. Gębicki, J. Romański, K. Jastrzębska, A. Sivaramamoorthy, K. Mason, D. H. Evans, M. Celeda and P. Kaszyński, *J. Org. Chem.*, 2013, **78**, 7445–7454.

16 S. Ciastek, K. Szymańska, P. Kaszyński and M. Jasiński, submitted.

17 For a recent indepth discussion of factors affecting EPR linewidth in paramagnetic liquid crystals see: A. K. Vorobiev, N. A. Chumakova, D. A. Pomogailo, Y. Uchida, K. Suzuki, Y. Noda and R. Tamura, *J. Phys. Chem. B*, 2014, **118**, 1932–1942.

18 M. J. Frisch, G. W. Trucks, H. B. Schlegel, G. E. Scuseria, M. A. Robb, J. R. Cheeseman, G. Scalmani, V. Barone, B. Mennucci, G. A. Petersson, H. Nakatsuji, M. Caricato, X. Li, H. P. Hratchian, A. F. Izmaylov, J. Bloino, G. Zheng, J. L. Sonnenberg, M. Hada, M. Ehara, K. Toyota, R. Fukuda, J. Hasegawa, M. Ishida, T. Nakajima, Y. Honda, O. Kitao, H. Nakai, T. Vreven, J. A. Montgomery Jr, J. E. Peralta, F. Ogliaro, M. Bearpark, J. J. Heyd, E. Brothers, K. N. Kudin, V. N. Staroverov, R. Kobayashi, J. Normand, K. Raghavachari, A. Rendell, J. C. Burant, S. S. Iyengar, J. Tomasi, M. Cossi, N. Rega, J. M. Millam, M. Klene, J. E. Knox, J. B. Cross, V. Bakken, C. Adamo, J. Jaramillo, R. Gomperts, R. E. Stratmann, O. Yazyev, A. J. Austin, R. Cammi, C. Pomelli, J. W. Ochterski, R. L. Martin, K. Morokuma, V. G. Zakrzewski, G. A. Voth, P. Salvador, J. J. Dannenberg, S. Dapprich, A. D. Daniels, O. Farkas, J. B. Foresman, J. V. Ortiz, J. Cioslowski and D. J. Fox, *Gaussian 09, Revision A.02*, Gaussian, Inc., Wallingford CT, 2009.